XVIII International Conference on Water Resources
CMWR 2010
J. Carrera (Ed)
CIMNE, Barcelona 2010

LARGE EDDY SIMULATION OF THE LOCK-EXCHANGE GRAVITY CURRENTS

Mani Mehdinia [1], Bahar Firoozabadi [2] and Mohammad Farshchi [3]

Sharif University of Technology (SUT), Tehran, Iran

[1] M.Sc. Student, Mechanical Engineering department, e-mail: mahdinia@mech.sharif.edu, web page: http://mech.sharif.edu/~mahdinia

[2] Associate Professor, Mechanical Engineering department, e-mail: firoozabadi@sharif.edu, web page: http://sharif.ir/~firoozabadi

[3] Associate Professor, Aerospace Engineering department, e-mail: farshchi@sharif.edu, web page: http://ae.sharif.ir/faculty-resume/farshchi.php

Key words: Turbulence, Dynamic large eddy simulation model, Lock exchange Gravity currents, Three dimensional models.

Summary: A code has been developed using the Dynamic Smagorinsky LES turbulence model to simulate the release of a finite-volume gravity current on a plane surface. Average concentration contours, front position, energy content time-evolution and the turbulence structure near the bed are presented and the effects of the lateral boundary conditions on these results are investigated. The results of the code are verified against experimental and numerical data. It has been shown that the local minimum-height points in the concentration contours are the points of the maximum near-wall turbulence intensity and that a narrow highly turbulent region forms near the nose of the current. It has also been demonstrated that the periodic lateral boundary condition results in less diffusion and mixing in the interface of the current, whereas the solid wall condition results in more uniformly distributed concentrations behind the head. Finally, it has been shown that the type of this boundary condition does not affect the longitudinal development of the current.

1 INTRODUCTION

Gravity currents are uniform currents, which move on a bed surface due to their higher density relative to the ambient and due to the gravitational force. Such a density variance can be originated from a temperature difference, chemical constituents or the solid particles, suspended in the current. These currents in general, may also be classified according to their type of initiation. In intrusion-type gravity currents, the heavy fluid enters from beneath a medium of lighter ambient fluid through a gate. The current then develops as it moves

forward on the surface. Examples of this kind of flow may be found in the simulations of Ooi et al. [1] and Hartel et al. [2,3]. The second kind of the gravity currents, which are studied in this article, are known as lock-exchange configuration currents. In this type, the heavy and light fluids are separated by a solid boundary (e.g. a vertical gate). As the gate is removed, each of the fluids intrudes into the other one. The volume of the heavier fluid may be finite or infinite, whereas the volume of the lighter one is generally infinite (its length is much larger than the height of the current). The simulations of Peik et al. [4] and Necker et al. [5] may be categorized in this group. The gravity currents may also be classified according to whether they contain particles or not. The work of Necker et al. [5] simulates particle laden flows, whereas the simulations of Peik et al. [4] and Ooi et al. [1] use the salt-water as the heavier fluid.

The initial arrangement of the finite-volume lock-exchange gravity current is presented in Figure 1. As shown by Herbert [6], the current travels through four distinct phases, as it propagates on the lower solid surface. In the first stage, the current gains velocity via the heavier fluid spreading over the bottom. After this short phase, the slumping phase ensues, where the current moves with a constant velocity. At the third stage, known as inertial phase, the velocity of the current begins to decrease. As suggested by its name, the inertial and buoyancy forces are balanced during this stage. Finally, in the viscous phase, the buoyancy force becomes balanced with the viscous force, and no more longitudinal development occurs. As the whole development of these stages requires a huge amount of time and also the turbulence characteristics of the current are of more importance in the initial stages, before their declination, the simulations in this article are continued to the end of the second phase, namely the slumping phase.

The gravity current has been studied both experimentally and numerically. Amongst the empirical works, are the experiments of Hacker et al. [7], Simpson [8], Ross et al. [9], Garcia [10], and Hallworth et al. [11]. The numerical methods have also been used extensively to study the gravity currents, but despite their high amount of value and the insight they give us, the majority of these works use the RANS turbulence models (like k-ε and k-ω), which only can calculate the mean characteristics of the flow and are not able to see the instantaneous fluctuations of the parameters like velocity and pressure. In this group, Stacy and Bowen [12] used the mixing length turbulence theory to determine the vertical structure of velocity and concentration in the currents. Eidsvik and Brørs [13] also used the Reynolds stress model to study the vertical structure of the current and Bournet [14] used the k-ε model to study the currents entering the reservoirs. The gravity current turbulence modeling using the LES and DNS methods has only become available recently and not much work has been done in this area. These methods, when compared to the conventional RANS techniques, are much more capable and sophisticated as will be shown in the text. The large eddy simulation works of Ooi et al. [1,15] and direct numerical simulations of Hartel et al. [2,3] and Necker et al. [5] are amongst the few works which may be categorized in the group of the works using more recent methods.

In the current article, the results of Hacker et al. [7] will be used as a base for the simulations. They investigate three different cases of finite-volume lock-exchange gravity currents. Here, we simulated the case B of their experiments. This case is the one with the highest Grashof number and thus is the most turbulent one. This arrangement has also been studied previously

by Ooi et al.[1] and Peik et al. [4] using the LES and *k-ε* models respectively. Here, we investigate some futures of the flow which have not been studied before, like the near-wall streaky turbulence structure and the effect of the lateral walls. We also compare the results of our simulations with the experimental data to verify the accuracy of the code and to examine its capabilities in predicating the flow properties.

2 GOVERNING EQUATIONS

The governing equations of motion are the continuity, momentum and concentration equations, which can be non-dimensionalized by using the buoyancy velocity $u_b = (g'H)^{1/2}$ and the initial lock height H (See Figure 1). Here, $g' = (\rho_{\max} - \rho_{\min})/\rho_{\min}$ is the corrected gravity and $\rho_{\max}$ and $\rho_{\min}$ are the initial densities of the heavier and lighter fluids, respectively. The non-dimensional resulting equations are

$$\frac{\partial u_k}{\partial x_k} = 0 \tag{1}$$

$$\frac{\partial u_i}{\partial t} + u_i \frac{\partial u_k}{\partial x_k} = -\frac{\partial p}{\partial x_i} + \frac{1}{\sqrt{Gr}} \frac{\partial u_i}{\partial x_k \partial x_k} + \frac{\partial}{\partial x_k}\left[2\nu_{SGS} S_{ik}\right] - C\delta_{i2} \tag{2}$$

$$\frac{\partial C}{\partial t} + u_k \frac{\partial C}{\partial x_k} = \frac{1}{\sqrt{Gr}\,Sc} \frac{\partial C}{\partial x_k \partial x_k} + \frac{\partial}{\partial x_k}\left[\alpha_{SGS} \frac{\partial C}{\partial x_k}\right] \tag{3}$$

In these equations, $S_{ik} = 1/2(\partial u_i/\partial x_k + \partial u_k/\partial x_i)$ is the instantaneous rate of strain, Gr is the Grashof number, Sc is the Molecular Schmidt number and ν_{SGS} and α_{SGS} are the Subgrid-scale viscosity and thermal diffusivity. Here, C denotes the non-dimensional concentration $(\rho - \rho_{\min})/(\rho_{\max} - \rho_{\min})$. A value of $Sc = 700$ is chosen for the molecular Schmidt number, according to the previous researches [1,4]. To close the equations above, the dynamic Smagorinsky model (originally developed by Lilly [16]) is used, so that the filtered stress $\tau_{ij} = \overline{u_i u_j} - \overline{u_i}\,\overline{u_j}$ (over-bar denotes grid-filtered and caret denotes test-filtered) resulting from the application of the grid filter to (2) can be modeled. The non-isotropic part of the grid and test filtered turbulence stresses are modeled as

$$b_{ij} = \tau_{ij} - \frac{1}{3}\delta_{ij}\tau_{kk} = 2C_s\Delta^2 |\overline{S}| \overline{S}_{ij} \tag{4}$$

$$B_{ij} = T_{ij} - \frac{1}{3}\delta_{ij}T_{kk} = 2C_S\hat{\Delta}^2 |\hat{\overline{S}}| \hat{\overline{S}}_{ij} \tag{5}$$

Where Δ and $\hat{\Delta}$ are the grid and test filter widths and τ_{ij} and T_{ij} are the grid and test filtered stresses, respectively. The dynamic model coefficient C_S, can then be found by applying the least square method (by minimizing the modeling error). The result is given by

$$C_s = 1/2(L_{ij}M_{ij} / M_{kl}M_{kl}) \tag{6}$$

The matrices L_{ij} and M_{ij} are given by

$$L_{ij} = -\widehat{u_i u_j} + \widehat{\overline{u}_i}\widehat{\overline{u}_j} \tag{7}$$

$$M_{ij} = \hat{\Delta}^2 |\widehat{\overline{S}}|\widehat{\overline{S}}_{ij} - \Delta^2 \widehat{|\overline{S}|\overline{S}_{ij}} \tag{8}$$

The use of the Dynamic LES model ensures an acceptable behavior of the current near the wall. The top-hat filter has been used for the grid and test filters and a test filter size of twice the grid filter size is used, which has been shown to give reasonable results previously [16]. Also the Van-driest damping function [17] was used on the filter sizes near the wall. To solve equation (3) for the concentration, the SGS diffusivity is calculated by a dynamic approach as suggested by Venayagamoorthy et. al. [18], so the turbulence Schmidt number and diffusivity are given respectively by

$$Sc_t = 0.4\exp(-2.5F_k) + 1.0 \tag{9}$$

$$\alpha_{SGS} = \nu_{SGS} / Sc_t \tag{10}$$

The turbulent Fraud number F_k in (9) and the buoyancy N are also given by

$$F_k = \varepsilon / Nk \tag{11}$$

$$N = \left(\frac{-g}{\rho}\frac{\partial \rho}{\partial z}\right)^{1/2} \tag{12}$$

Where ε and k are the turbulence dissipation rate and kinetic energy, respectively.

3 SOLUTION TECHNIQUE

To descritize the flow equations, the QUICK algorithm has been used for the divergence and laplacian terms. The Gradient term on the other hand is descritized by a fourth order central scheme as described by Peer et al. [19]. The temporal term is also descritized by a second-order backward method. The resulting equations are solved by the preconditioned biconjugate gradient method with the Diagonal incomplete LU asymmetric priconditioner. The iteration process is repeated for each equation until the error falls below 10^{-5}.

4 SOLUTION DOMAIN AND BOUNDARY CONDITIONS

The computational domain and its boundary conditions are shown in Figure 1. The far-left boundary is modeled as a solid wall, whereas the outflow boundary, to the right of the domain is taken to be a convective outflow boundary, as was used by Pierce and Moin [20] before. The upper boundary is a zero-shear surface and the bottom surface incorporates a no-slip boundary condition. The front and back boundaries in the figure are labeled as solid walls, but actually

two simulations are carried out. In the first, we use wall condition for lateral walls and in the second a periodic boundary condition is incorporated. These cases are labeled as B and Bc in the article. The domain in Figure1 pertains to case B of the experiments of Hacker et al. [7].

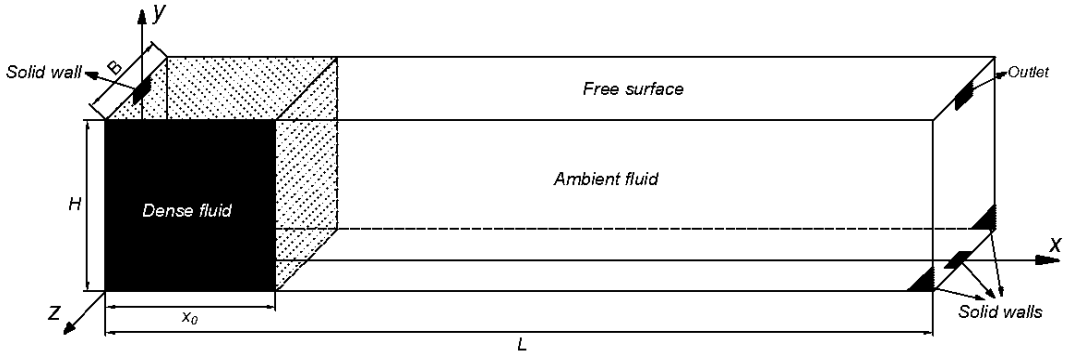

Figure 1: The initial configuration of the finite-volume lock-exchange gravity current

A mesh size of 400×80×80 is used for the modeling of the flow in x, y and z directions respectively. The mesh size near the wall is such that a value of $y^+ = 20$ is achieved, so the wall functions are used for the near-wall modeling. The size of the domain in the longitudinal direction is $L / x_0 = 5$, which covers the entire range of the existing empirical results. A time interval of 0.005 sec is used, so that the maximum Courant number reaches a value of less than 0.25. The solution is carried out till 14.0 sec, which is the end of the slumping phase. The current has a Fraud number of $u_f / u_b = 0.45$ (u_f is the speed of the front during the slumping phase) and a corrected gravity of $g' = 0.12$. The value of the Grashof and Reynolds numbers are $Gr = (u_b H / \nu)^2 = 7.7 \times 10^9$ and $\mathrm{Re} = u_b H / \nu = 19700$, respectively.

5 SIMULTION RESULTS

5.1 Verification

The depth-averaged concentration contours for case B are compared with the experimental results in Figure 2. The time $t_0 = H / u_b$ has been used to non-dimensionalize the times. As can be seen, there is a good agreement between the numerical and experimental contours, especially at the later times. There is a slight difference between the results in the initial moments. The reason for this is the finite speed of the gate in the experiments, which causes the empirical contours to be non-symmetric initially. In the LES results on the other hand as can be seen by the figure, the pattern is much more symmetric due to the instantaneous removal of the gate. The disturbances produced by the removal of the gate at the upper surface also acts as a means to decline the symmetry. Such an inconsistency was previously seen by the other researchers too [1,4]. Since these contours have previously been examined by other researchers, we move forward to present other results of our work.

5.2 Streaky near-wall turbulence pattern of the flow

The velocity fluctuation and the corresponding concentration contours on the first grid off the wall (y^+=20), are shown in Figure 3. As can be perceived, the mean speed of the current is nearly zero in the vicinity of the wall, these diagrams then show the intensity of the local turbulence.

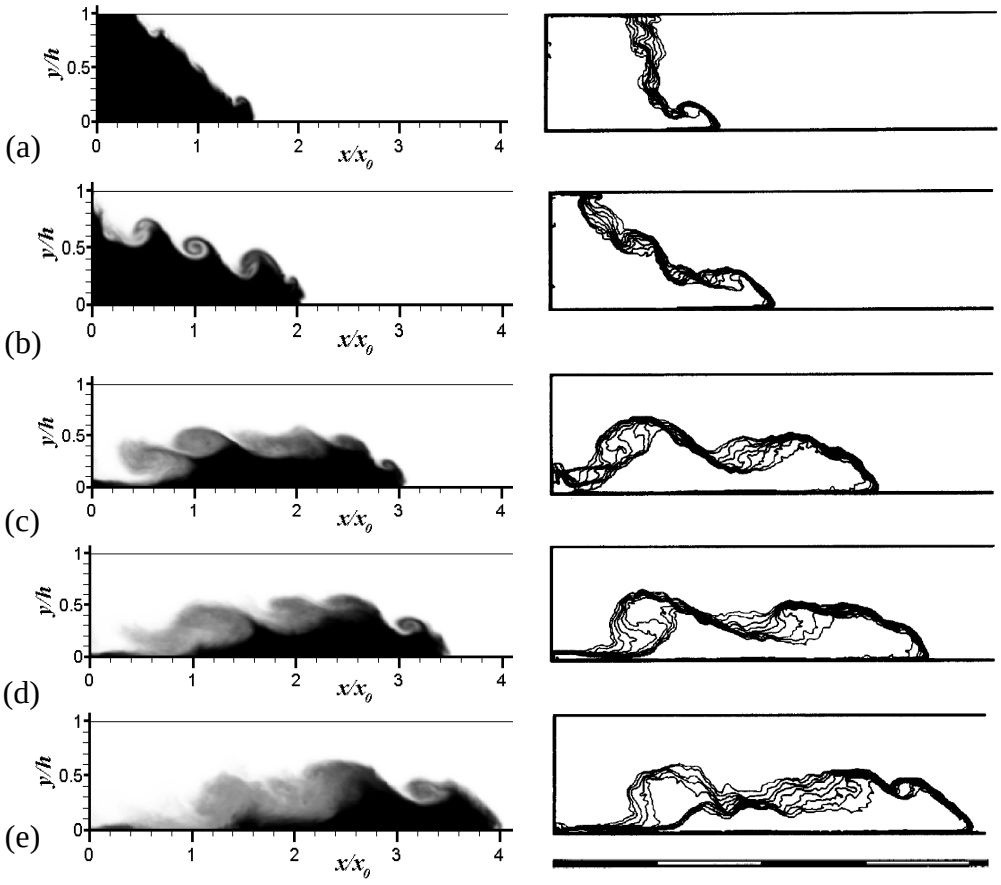

Figure 2: Experimental [7] (right) and numerical case B (left) depth averaged concentration contours at (a) $t/t_0 = 1.4$ (b) $t/t_0 = 2.4$ (c) $t/t_0 = 4.6$ (d) $t/t_0 = 5.6$ (e) $t/t_0 = 6.6$

At the nose position of the head, there is a narrow band of high intensity turbulence. Hartel et al. [2,3] have previously demonstrated by their DNS results, that the near nose region of the current is the place where the instabilities leading to lobe and cleft structure occur. This is in agreement with the narrow but highly turbulent band in Figure 3. Behind the front there exists a series of high and low intensity bands, across the longitudinal dimension of the current. To describe these areas, one might consider the corresponding concentration contours at each time. As the current moves on the lower surface, the Kelvin-Helmholtz instabilities, force the heavier fluid underneath the ambient to form some local minimum and maximum points in

the concentration distribution. According to the continuity law, the points of minimum heavy fluid height correspond to the larger velocities across the lower fluid and vice versa. This assumption can be proved by investigating figure 4, which shows the depth-averaged instantaneous velocity of the current, at some distance from the bed (not as small as the distance of the velocity contours in Figure 3). For instance, there is a maximum and a minimum velocity point at $x/x_0 = 3$ and $x/x_0 = 2.6$ at $t/t_0 = 5.6$ in Figure 4, which correspond to the local high-concentration minimum and maximum heights in Figure 3(b), respectively. Since in the minimum-height points the velocity increases, this results in an increase in the value of the local Reynolds number and this in turn gives rise to higher turbulence intensities. All this discussion shows that the minimum points of the heavy lock height correspond to the maximum points of the turbulence intensity contour and vice versa.

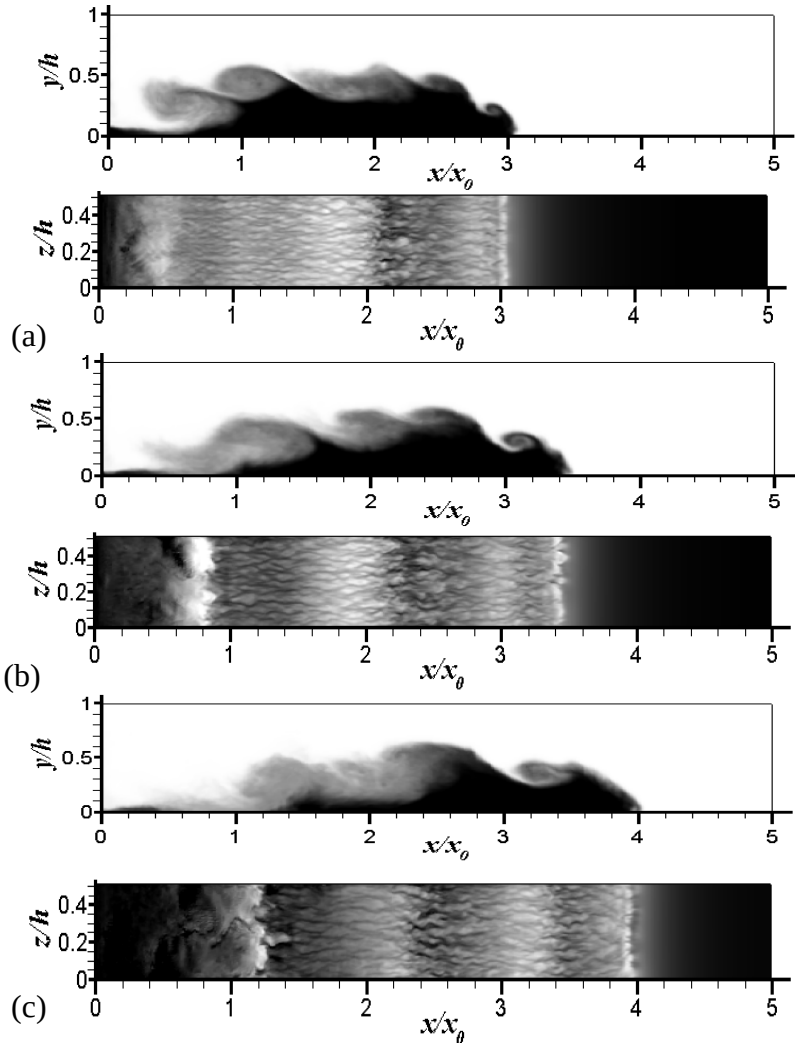

Figure 3: Streamwise velocity fluctuation and the corresponding depth-average concentration contours at y^+=20 near the bottom wall for case B at (a) $t/t_0 = 4.6$ (b) $t/t_0 = 5.6$ (c) $t/t_0 = 6.6$

Behind this longitudinally varying turbulence, a nearly uniform streak-free part can be seen. This high velocity region pertains to the Kelvin-Helmholtz instabilities in the tail becoming in contact with the lower bed, due to the removal of the high density lock. After this part, there comes a turbulence-free and zero velocity part, which occurs due to the settling of the high-density current over the bed. The length of this region increases as the current moves forward on the surface

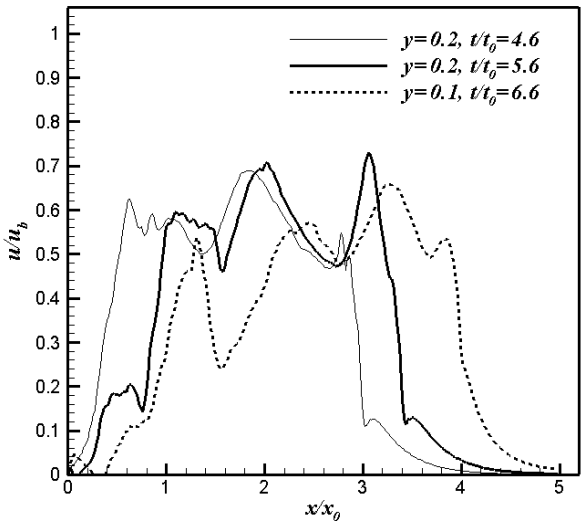

Figure 4: Depth-averaged velocity contours at different elevations from the bed and at different times

To our knowledge, such a description about the near-wall turbulence structure of the lock-exchange density currents has never been carried out before.

5.3 Effect of the boundary conditions

The simulation of the Hacker et al. [7] experimental studies has previously been carried out by Ooi et al. [1] and Peik et al. [4]. The first of these uses an LES method with periodic lateral boundary condition whereas the second one uses an enhanced *k-ε* method and the wall condition for the lateral boundaries. None of these works investigates the effect of the front and back boundary condition on the development of the current and its parameters. Here, by running a case for periodic conditions (case Bc) we investigate this effect.

Figure 5 shows the front position data for cases B and Bc. As can be seen from the figure, the lateral boundary condition does not change the rate of the horizontal development of the current. Figure 5 also shows the evolution of the various energy sources of the current with time. The energy contents shown, include the dissipation E_d, the potential E_p and the kinetic E_k energies of the current and are non-dimensionalized by the initial potential energy E_{p0}. These are calculated by the procedure outlined by Necker et al. [5], who show that if the velocity components are zero on all of the boundaries of the system (except the outlet) and the effect of dissipation in the concentration transport equation can be neglected, then the sum of these three sources remains constant. By inspecting Figure 5, it can be concluded that this is also

the case here. As the current develops on the surface its potential energy decreases and its kinetic energy increases. This procedure continues till $t/t_0 = 3.8$, where the effects of the dissipation becomes significant and both energies begin to decline. The effect of the wall boundary condition can't be seen until $t/t_0 = 3.8$. After this moment, the wall BC in case B produces so much dissipation that the rate of decrease of the potential and kinetic energies decreases relative to the case Bc.

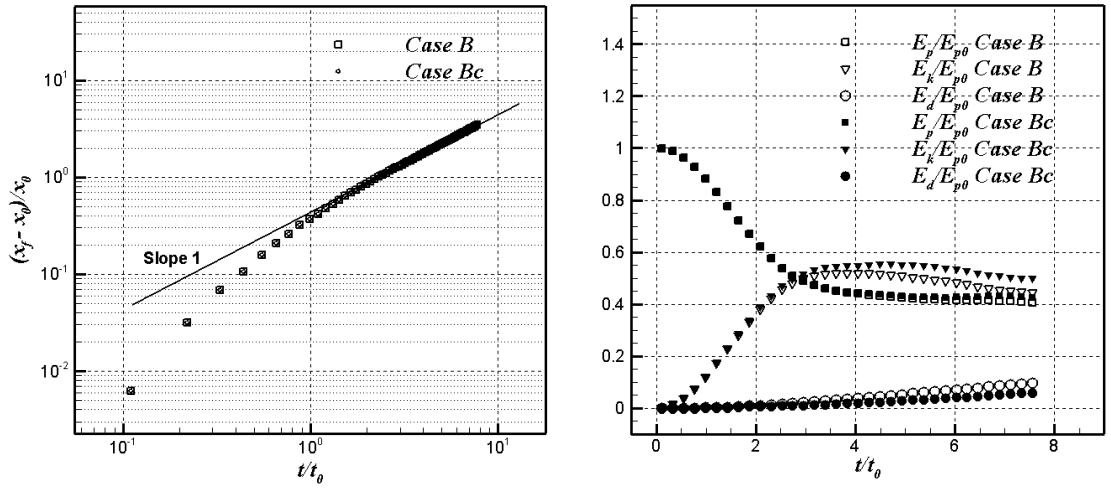

Figure 5: Front position (left) and energy content (right) of the current for cases B and Bc

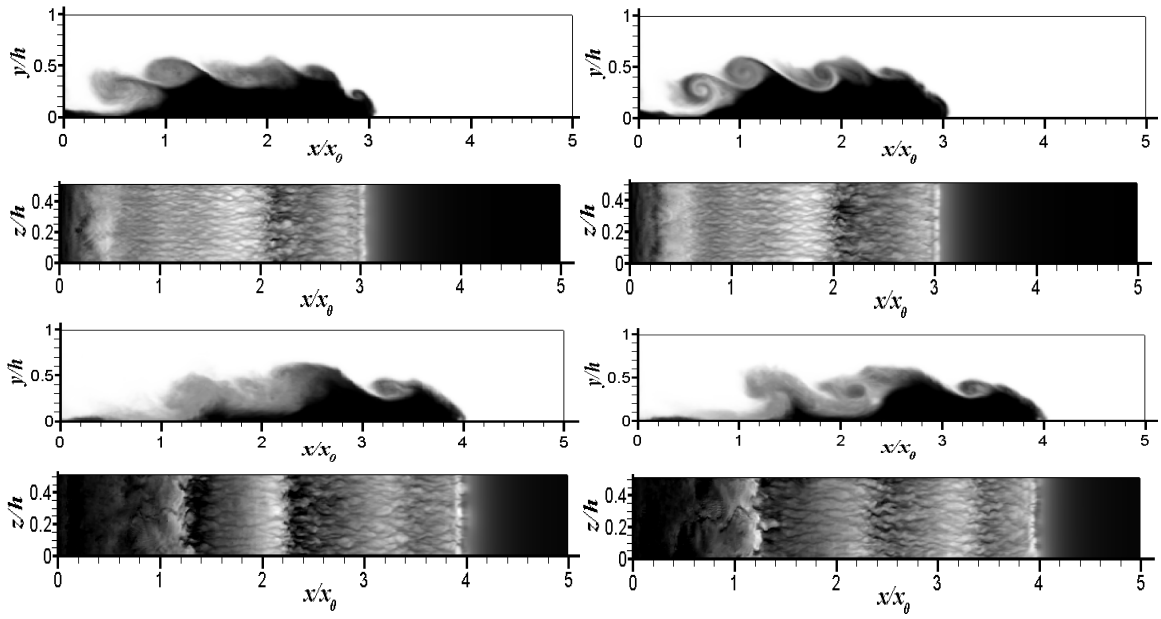

Figure 6: Streamwise velocity fluctuation and the corresponding depth-average concentration contours at y^+=20 for case B (left) and case Bc (right) at (a) $t/t_0 = 4.6$ (b) $t/t_0 = 6.6$

The effect of the lateral BC on wall turbulence structure and concentration contours is shown in Figure 6. As can be seen, the wall condition results in more mixing and diffusion in the current, such that the average concentration contours in this case become smeared, specially in the locations of the Kelvin-Helmholtz instabilities, while the vortexes keep their identity for a longer time in the case of the periodic boundary condition. The turbulence structure is also more three dimensional (in the mean sense) for the wall case.

It should be mentioned that since the lateral BC does not effect the longitudinal progress of the current, so the effects of this BC remains in a small distance from the wall, at least for the simulation length considered here.

6 CONCLUSIONS

Using the dynamics LES model, the gravity currents developing on a plane surface has been studied. It has been shown that the streaky turbulence pattern of the flow velocity near the bed is a measure of the turbulence intensity of the flow and that the local minima and maxima of the depth-averaged concentration profiles are the regions of high and low turbulence fluctuations respectively. It has also been shown that there are two highly turbulent regions in the front and tail part of the current and after the current has passed a point, eventually the turbulence is damped and the fluctuations drop to zero after sufficient amount of time.

The effect of the lateral boundary conditions has also been investigated on the development of the flow. According to the LES results, the wall BC results in more dissipation and diffusion of the flow and renders the interfacial region more uniform. On the other hand, with the periodic boundary conditions the Kelvin-Helmholtz instabilities remain more concentrated as they are shed at the interface. The wall boundary condition results in a more three-dimensional current than does the periodic condition.

7 REFERENCES

[1] S. K. Ooi, G. Constantinescu and L. Weber, “Numerical simulations of lock-exchange compositional gravity current”, *J. Fluid Mech.,* **635**, 361-388 (2009).

[2] C. Hartel, F. Carlsson and M. Thunblom, “Analysis and direct numerical simulation of the flow at a gravity-current head. Part 2. The lobe-and-cleft instability”, *J. Fluid Mech.*, **418**, 213–229 (2000).

[3] C. Hartel, E. Meiburg and F. Necker, “Analysis and direct numerical simulation of the flow at a gravity-current head. Part 1. Flow topology and front speed for slip and no-slip boundaries”, *J. Fluid Mech.*, **418**, 189–212 (2000).

[4] J. Paik, A. Eghbalzadeh and F. Sotiropoulos, “Three-Dimensional Unsteady RANS Modeling of Discontinuous Gravity Currents in Rectangular Domains”, *J. Hyd. Eng.*, **135**, 505-521 (2009).

[5] F. Necker, C. Hartel, L. Kleiser and E. Meiburg, “Mixing and dissipation in particle-drive gravity currents”, *J. Fluid Mech.*, **545**, 339–372 (2005).

[6] H. E. Herbert and J. E. Simpson, "The slumping of gravity currents", *J. Fluid Mech.*, **99**, 785–799 (1980).
[7] J. Hacker, P. F. Linden and S. B. Dalziel, "Mixing in lock-release gravity currents", *J. Dyn. of Atmos. and Oceans*, **24**, 183-195 (1996).
[8] J. E. Simpson, "Effects of the lower boundary on the head of a gravity current", *J. Fluid Mech.*, **53**, 759-768 (1972).
[9] A. N. Ross, P. F. Linden and S. B. Dalziel, "A study of three-dimensional gravity currents on a uniform slope", *J. Fluid Mech.*, **453**, 239-261 (2002).
[10] M. H. Garcia, "Hydraulics jumps in sediment driven bottom currents", *J. Hyd. Eng. ASCE*, **119**, 1094-1117 (1993).
[11] M. A. Hallworth, H. E. Huppert, H. E. Phillips and R. S. J. Sparks "Entrainment into two-dimensional and axisymmetric turbulent gravity currents", *J. Fluid. Mech.*, **308**, 289-311 (1996).
[12] M. W. Stacey and A. J. Brown, "The vertical structure of turbidity currents and a necessary condition for self-maintenance", *J. Geo. Research*, **93**, 3543-3553 (1988).
[13] K. J. Eidsvik and B. Brørs, "Dynamic Reynolds stress modeling of turbidity currents", *J. Geo. Research*, **97**, 9645-9652 (1992).
[14] P. E. Bournet, D. Dartus, B. Tassin, B. Vincon-Leite "Numerical investigation of plunging density current", *J. Hyd. Eng. ASCE*, **125**, 584-594 (1999).
[15] S. K. Ooi, G. Constantinescu and L. J. Weber, "2D Large-Eddy Simulation of Lock-Exchange Gravity Current Flows at High Grashof Numbers*", J. Hyd. Eng. ASCE*, **133**, 1037-1047 (2007).
[16] D. K. Lilly, "A proposed modification of the Germano subgrid-scale closure method", *Phys. of Fluids*, **4**, 633-635 (1992).
[17] P. Moin and J. Kim "Numerical investigation of turbulent channel flow", *J. Fluid Mech.*, **118**, 341-377 (1982).
[18] S. K. Venayagamoorthy, J. R. Koseff, J. H. Ferziger and L. H. Shih "Testing of RANS turbulence models fro stratified flows based on DNS data", *Cnt. of Turb. Research annual research briefs*, Stanford Univ., 127-138 (2003).
[19] A. A. I. Peer, A. Gopaul, M. Z. Dauhoo and M. Bhuruth, "A new fourth-order non-oscillatory central scheme for hyperbolic conservation laws", *App. Num. Mathematics*, **58**, 674-688 (2008).
[20] C. D. Pierce and P. Moin, "Progress-variable approach for large eddy simulation of turbulent combustion", *Rep. TF-80, Mech. Eng. Department, Stanford Univ.*, (2001).